Lab on a Chip

PAPER

View Article Online
View Journal | View Issue

Cite this: *Lab Chip*, 2020, **20**, 3784

Needle-free delivery of fluids from compact laser-based jet injector

Jan Krizek, * Frédéric De Goumoëns, Paul Delrot and Christophe Moser

Jet injection devices have been studied and developed for transdermal drug delivery to avoid the use of needles. Due to bulky actuation mechanisms, they are limited to body areas that are easy to reach such as skin. Here, we demonstrate a thin and long liquid delivery system (*e.g.* flexible and 30 cm long with 1.2 mm outer diameter) compatible with minimally invasive surgical procedures. The actuation mechanism is based on optical cavitation in a capillary nozzle where a laser pulse is delivered *via* a multimode optical fibre. We show good controllability of the jet speed by varying the actuation laser fluence. The generated jets can successfully penetrate into a 1% agarose gel which is representative of the mechanical properties of several soft body tissues. We further observe that when the system is used in a low laser energy regime (<60 μJ), the ejection is in the form of the single droplet which is promising for fluid delivery with high volume precision or drop-on-demand inkjet printing. The jet injection system we propose has the potential to deliver heat-sensitive therapeutics as we show processing of biomolecules without altering their functionality.

Received 22nd June 2020,
Accepted 1st September 2020

DOI: 10.1039/d0lc00646g

rsc.li/loc

1. Introduction

Technologies that can precisely deliver drugs in a spatially confined inner body environment are highly relevant for various fields in medicine such as deep brain stimulation,[1,2] inner ear treatment,[3] ophthalmology[4,5] or various targets of gene or photodynamic therapy.[6–10] Here, we present a device based on jet-injection technology in the long and thin embodiment as the alternative to address both challenges of the system miniaturisation and the precision of the drug dose delivery.

Jet-injection techniques for transdermal vaccination were introduced to overcome issues associated with hypodermic needles.[11] Such contactless devices provide better dose control, lateral and depth localization and lower collateral damage than the needles.[12,53] In needle-free injection devices, the liquid is pushed out of the nozzle forming a thin jet, which is powerful enough to penetrate into a tissue. The actuation scheme is commonly based on a piezoactuator,[13–15] loaded spring,[11,16] gas cartridge,[11] voice coil actuator[17,18] or an electrical discharge.[5,19,20] These actuation mechanisms are bulky and do not allow implementation as a compact minimally invasive device. Even if miniaturization could be performed, it would pose a safety concern about bringing high voltages or high pressure elements inside the body.

Laser induced cavitation has been investigated as the driving mechanism for needle-free injection systems.[12,21–30] Tagawa *et al.*[28] demonstrated injection with a new type of highly focused liquid microjets generated by a laser pulse focused by an optical objective from the side of a transparent nozzle. In the recent study by Krizek *et al.*[29] this concept was elaborated on hydrogel models mimicking stiffer materials representing mechanical properties of various soft body tissues up to 0.5 MPa (*e.g.* cancer tissue). Here we demonstrate technical advancement in the design allowing miniaturisation step in the form of a long and thin delivery device by bringing the optical pulse from within the capillary as opposed to the side. Using optical fibres to deliver light unfolds the potential of using optical energy as a driving mechanism. The fact that the energy can be remotely generated in a large laser system and then delivered by means of very thin fibres is convenient for miniaturization the jet delivery device. A device employing optical fibres has multiple advantages compared to those using free space optics to focus light from the side of the capillary, as previously reported in the literature.[25,28,29,31,32] First of all, the systems with a side focusing lens are not compact and do not allow implementation into hand-held or minimally invasive device. In addition, ensuring reproducible jet ejection requires a fine alignment of the position of the capillary with respect to the focusing lens. On the contrary, in the proposed system with the optical fibre, the light delivery is at the tip of the fibre, whose position is centred in the capillary by design. Moreover, the nozzle material is

School of Engineering, Swiss Federal Institute of Technology in Lausanne (EPFL), Station 17, 1015 Lausanne, Switzerland. E-mail: jan.krizek@epfl.ch

limited to transparent glass capillaries whereas the fibre-based system can easily work with standard metal syringes.

In this manuscript, we report on the design and performance of a fibre-based jet-injection device actuated by laser-induced cavitation. We demonstrate applicability for needle-free injection on 1% agarose gels mimicking mechanical properties of soft tissues. Furthermore, we show the generation of a slow speed single droplet with parameters suitable for low volume (nl) drug delivery or for drop-on-demand printing. We investigate the impact of laser fluence and the distance of the fibre tip to the liquid meniscus on jet velocity. We also show jet generation with common non-aqueous solvents relevant to injectable drugs – oil, glycerol and ethanol. Finally we show that the ejection mechanism did not denature the molecules contained in the liquid.

2. Materials and methods

2.1. Jet generation

Laser-actuated liquid microjets from capillaries have been pioneered by Lohse *et al.*[32,33] Energy from the laser pulse leads to optical breakdown in the fluid followed by the rapid expansion of a vapor bubble which is growing towards the liquid/air meniscus interface. The axisymmetric curvature of the meniscus results in the local orientation of the pressure gradient towards the centre and forms a geometrically highly focused and further accelerated flow. The generated jet has a needle-like shape and despite its high Reynolds number (the highest measured Re $\approx 10^4$), the jet-tip sustains its shape during the propagation.

2.2. Set-up

The experimental setup is described in Fig. 1, 5 ns laser pulses are emitted by a Q-switched laser source (Continuum, ML-II, 532 nm). Laser pulses are split by a polarization beam splitter and monitored by an energy meter (Thorlabs, ES111C). Light is further coupled into a multimode optical fibre with core diameter varying from 200 μm, 105 μm and 50 μm (ThorLabs, FG200LEA, FG105LCA, FG050LGA). The fibre is inserted into a round capillary that has 0.3 mm inner diameter and 1.2 mm outer diameter (see Fig. 2a), and which is filled with the injection liquid. The capillary's length is 9.5 cm in the experiment, but it could be longer or shorter depending on the application. The tool is not limited to the rigid nozzle but can be also embodied with a flexible Teflon tubing (Fig. 2b) and a glass capillary nozzle on the tip. Flexibility is limited by the ability of the optical fibre to guide the light without leaks. To connect the optical fibre with the liquid supply shaft, we use a T-junction (Upchurch, Scientific MicroTees). Handling of the fluid and the meniscus positioning is performed by a hand-controlled syringe pump. The experiment is monitored with an ultra-fast camera (Vision Research, Phantom Miro M310). The minimum time between two frames in our experiments is set to 10 μs (100 kfps). The time synchronization of the laser pulse and the camera is performed by a delay generator (Berkeley

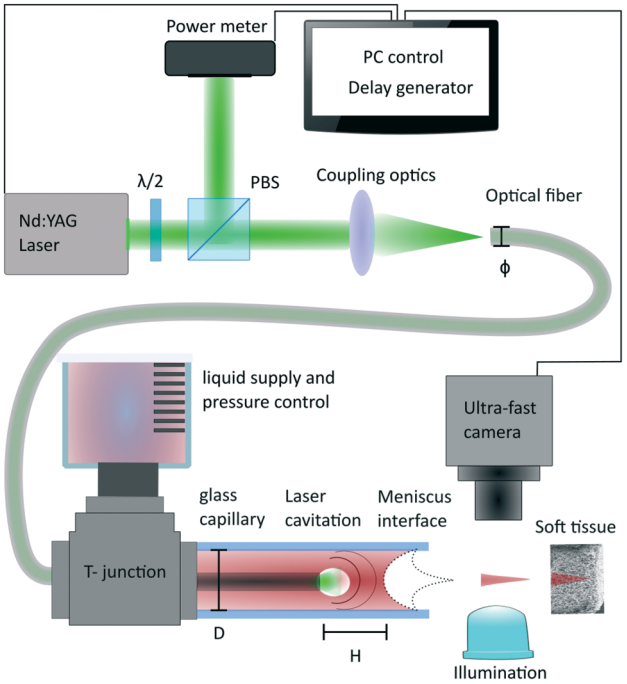

Fig. 1 Scheme of the experiment. The generated laser pulse is coupled into the optical fibre. The fluid and optical fibre channel are connected in the T-junction which is further plugged into the glass capillary. The jet generation, its velocity and injection into gel phantoms is monitored by the ultrafast camera. *D* – capillary diameter, *H* – fibre end to meniscus distance, ϕ – fibre core diameter.

Nucleonics, Model 577). The agarose gel for the tissue phantom was prepared by dissolving 1 g of the agarose powder (Sigma-Aldrich, Germany) in 100 ml of deionized water. Hydrogel substrates were used in the same day within about 2 hours after gelation. Parameter measurements are made with the stained DI water with 52 mM of Allura Red AC (ARAC; 80%, Sigma Aldrich, USA) to enhance the absorption of the light. Demonstration of non-aqueous jets were made on following formulations: sunflower oil (Migros France SAS) was stained to a dye concentration of 56 mM oil red EGN (Aldrich, USA). Glycerol was stained with 52 mM Allura Red

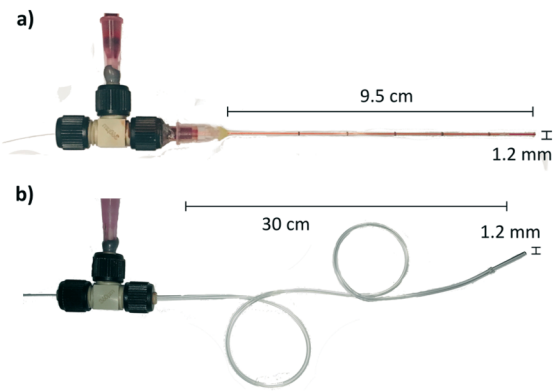

Fig. 2 Example of the tool embodiment. a) Rigid glass capillary 9.5 cm long and 1.2 mm thin; b) flexible Teflon tube with a glass capillary tip, 30 cm long, 1.2 mm thin.

(ARAC; 80%, Sigma Aldrich, USA). Ethanol was stained with 52 mM Allura Red (ARAC; 80%, Sigma Aldrich, USA).

2.3. Fibre coupling and laser induced damage threshold

The pulse energy that can be transmitted by the optical fibre is limited by the damage threshold of the fibre glass media. Spatial confinement of the laser pulse into the narrow fibre core leads to high power densities and consequently induced non-linear effects.[34,35] The laser induced damage threshold (LIDT) determines the maximum fluence (J cm^{-2}) the fibre can handle. For a wavelength λ = 532 nm, and pulse duration τ = 5 ns the theoretical estimation is 50 J cm^{-2}. This is estimated considering a flat top energy distribution at the end of fibre facet. Experimentally, we observe that the minimum fluence sufficient for the liquid cavitation is in the range of 0.5–1 (J cm^{-2}), which is 50 to 100 times lower than the glass damage threshold. It must be noted that the cavitation threshold strongly depends on the fluid absorbance for a given wavelength.

2.4. Immunoassay protocol

Compatibility test of the system for processing heat-sensitive molecules was made by assessing the integrity of rabbit immunoglobulin (IgG) following the protocol described in ref. 36 or in ref. 31. The rabbit IgGs (IgG; Sigma-Aldrich, Germany) are diluted at a concentration of 50 ng μl^{-1} in 80% (v/v) PBS (PBS; Gibco®, Thermo-Fisher Scientific, UK) and 20% (v/v) of glycerol. Further staining was made by 52 mM of Allura Red AC (ARAC; 80%, Sigma Aldrich, USA). The solution containing IgG is deposited and dried onto poly-L-lysine slides (Sigma Aldrich, USA) to assure the adhesion of the molecules to the substrate. Further, slides are blocked with 3% (w/v) bovine serum albumin (BSA, Sigma Aldrich, USA) for 30 min to avoid unspecific bonding of the secondary antibody. Then, they are washed three times with the solution of 0.1% (v/v) Tween-20 (PBS-T; Sigma Aldrich, France) in PBS. In the next step we perform an immunoassay by incubating for 30 min in a 30 ng μl^{-1} solution of secondary antibodies against rabbit IgG (Cy3-AffiniPure anti-rabbit IgG, Jackson Immunoresearch, UK) conjugated with fluorescent labeling. Slides are further washed three times by the PBS-T, once with the DI water and once in 96% (v/v) ethanol. Fluorescent imaging is made by a microscope (Leica DM5500).

3. Results and discussion

3.1. Parameter dependence

The study of Tagawa *et al.*[32] gives good insights of the jet-generation parameter space. In their study, the relationship:

$$v_{jet} \propto (1 + \beta \cos\theta)\frac{(E - E_{heat})}{D{\cdot}H}$$

is established between the jet velocity v_{jet}, the absorbed laser energy E, the capillary diameter D, the distance between the meniscus and the laser focus H and the curvature angle of the air–liquid interface θ. Here, we further introduce the parameter S describing the area on which the laser energy is distributed $v_{jet} = f(S, E, H, D, \beta\cos\theta)$. In our fibre-based jet injection device, the focusing area is well defined within the fibre as opposed to the previous works in which a side illumination was used to focus light. We experimentally observe a clear dependence of the jet velocity on the area S as described in the next section.

3.1.1. Laser energy and fluence. It was shown by Tagawa *et al.*[32] that the jet velocity is a linear function of absorbed energy. We measured the jet velocity for three different optical fibre core sizes (50, 105, 200 μm) while keeping the same distance of the fibre end from the meniscus (Z = 300 μm), the same capillary size (D = 300 μm), the same meniscus curvature and a constant delivered energy. We obtained jet velocities that depend on the fibre core diameter, as illustrated in Fig. 3. This suggests that there is another parameter to consider which is related to the area of the energy deposition, or in other words to the laser fluence (J cm^{-2}). This is also in agreement with literature focusing on laser cavitation phenomena in fluids.[37–39]

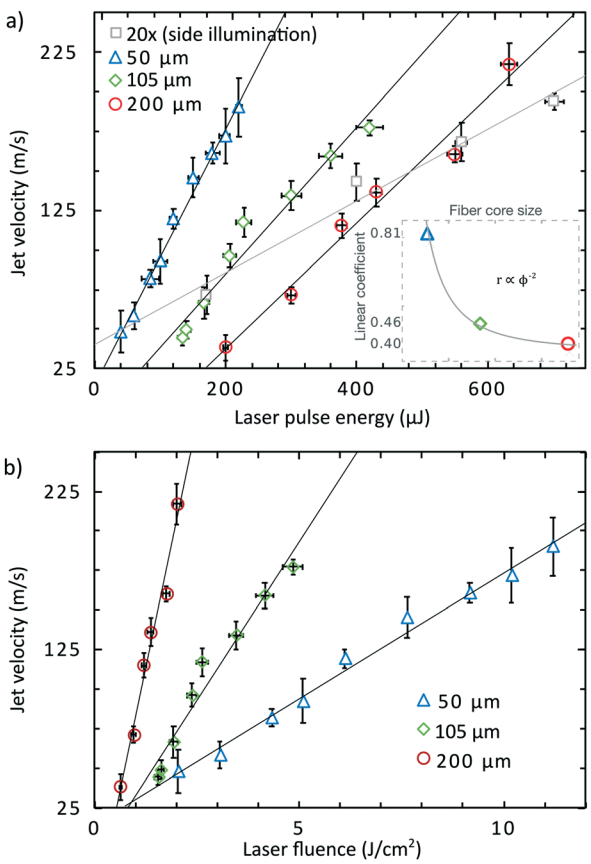

Fig. 3 Velocity of the jet in dependence of the a) energy and b) laser fluence (energy density). Capillary diameter 300 μm, fibre end is positioned 300 μm apart from the meniscus. Error bars are standard deviation from at least 5 measurements. Equation of linear trendlines for 50, 105, 200 μm fibre and 20× objective are following: v_{50} = 0.81E + 15, v_{105} = 0.46E − 8, v_{200} = 0.40E − 42, v_{20x} = 0.23E + 40.

The correlation coefficients of linear regressions (r) from the Fig. 3a and the fibre core size diameter ϕ can be fitted by the function $r \propto \phi^{-2}$, which is in good agreement to the definition of the laser fluence. Smaller fibre cores give rise to higher fluences therefore with the same amount of energy, the jet velocity is higher for smaller core fibre. On the other hand, a smaller fibre core is not able to transport as much total energy as a larger core fibre because of the laser induced damage threshold of the fibre. The graph in Fig. 3b shows the jet velocity as a function of the laser fluence. It shows that the fluence nor energy cannot be used as a single parameter to determine the resulting jet speed as it also depends on the fibre core. Thus, the integral energy has to also be considered. We suggest to modify the relation for the liquid jet velocity v_{jet} in ref. 32 by adding the parameter S – the area on which the laser light is focused:

$$v_{jet} \propto S^{-1}$$

Interestingly, when we compare the jet velocity obtained with a side illumination set-up (same experimental parameters with a 20× microscope objective for side illumination as in ref. 32), grey square marker in Fig. 3a), we see a lower jet velocity increase with laser energy than when the optical fibre is used in the capillary. This can be explained as follows: the laser focus from the objective creates an energy density higher than the laser induced damage threshold of the glass capillary, thus to avoid capillary breakage, the focal point has to be shifted towards the center of the capillary, which gives a larger illumination area at the interface between the capillary wall and the liquid. This defocus yields a lower fluence and results in lower jet velocity.

3.1.2. Distance *H*. The dependence of the jet velocity on the distance between the vapor bubble and the meniscus interface was modelled as ($v_{jet} \propto H^{-1}$) from ref. 32 and 33. The vapor bubble generated with the objective is always located at the capillary wall interface where the energy is mainly absorbed because of the staining of the ink. This geometrical offset from the central axis of the capillary causes a tilted jet when we focus the light closer than the D capillary diameter. This is not the case with the fibre actuation for which the cavitation happens in the centre of the capillary by design. With this arrangement, we can generate straight jets with a meniscus to bubble distance smaller than the capillary diameter. Fig. 4 depicts the dependence of the jet velocity on the distance between the fibre-end and the meniscus for distances shorter than the capillary diameter. The experimental data is fitted to a linear dependence, $v_{jet} \propto -rH$. For distances lower than ≈ 100 μm we observed splashing rather than a focused jet.

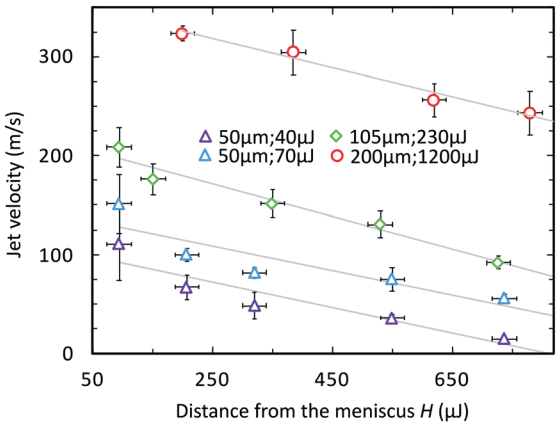

Fig. 4 Velocity of the jet on the actuation distance from the meniscus. Capillary diameter 300 μm, fibre end is positioned 300 μm apart from the meniscus. Error bars are standard deviation from at least 5 measurements. Linear fit equation are following: $v_{200} = -0.15H + 355$, $v_{105} = -0.17H + 213$, $v_{50} = -0.13H + 105$.

3.2. Jet injection

In the previous study, Tagawa *et al.*[28] shows successful penetration through the skin. The dynamics of penetration into gels is also further studied in ref. 25, 29 and 40. A more exhaustive evaluation of injection capability into various material stiffnesses was demonstrated in ref. 29. We expect these results would be the same as the features of the jet such as shape and velocity distribution remains the same. Applicability of our device for jet injection was tested on a 1% agarose gel which is commonly used as a human skin phantom to investigate performance of needle-free injection device.[20,41,42] One characteristic feature of focused jets is the unequal velocity distribution along the jet. The front part has a larger velocity than the following slow tail. On Fig. 5, we can see three examples of injection sequence with different distances of the fibre to the meniscus but with the energy level tuned so that the velocity is around 130 m s^{-1}. In the first case, the actuation happens at a distance of 150 μm from the meniscus: we observe that the whole ejected liquid volume is subjected to the flow focusing effect and the slow tail is mitigated. The injection efficiency is therefore high (>94%). (Calculation of injection efficiency is based on the portion of the jet entering the hydrogel.) The volume of injected fluid is around 14 nl. The second example shows the actuation at a distance of 300 μm – the focused part is followed by a slower tail (60 m s^{-1}) which still have sufficient power to penetrate in the gel. The injection efficiency is lower than in the former case (>86%), but the injected volume is augmented. The total volume ejected is approximately 24 nl. In the last example, the actuation site is located 680 μm away from the meniscus, value is representing 2-times diameter of the nozzle – the distance used in systems with the side illumination.[25,29,40] We observe that a considerable amount of the ejected liquid is contained in the slow tail which does not have a sufficient velocity (43 m s^{-1}) to penetrate into the gel and it is bounced off the surface (Fig. 5, H = 680 μm, at 203 μs). The total ejected volume is 48 nl, but considering that only the focused part entered the gel, the injected volume is similar to the first case, but yielding an injection efficiency of approximately 30%. There is thus a trade-off between injection efficiency and injection volume with a single shot. The total volume can be also adjusted by using

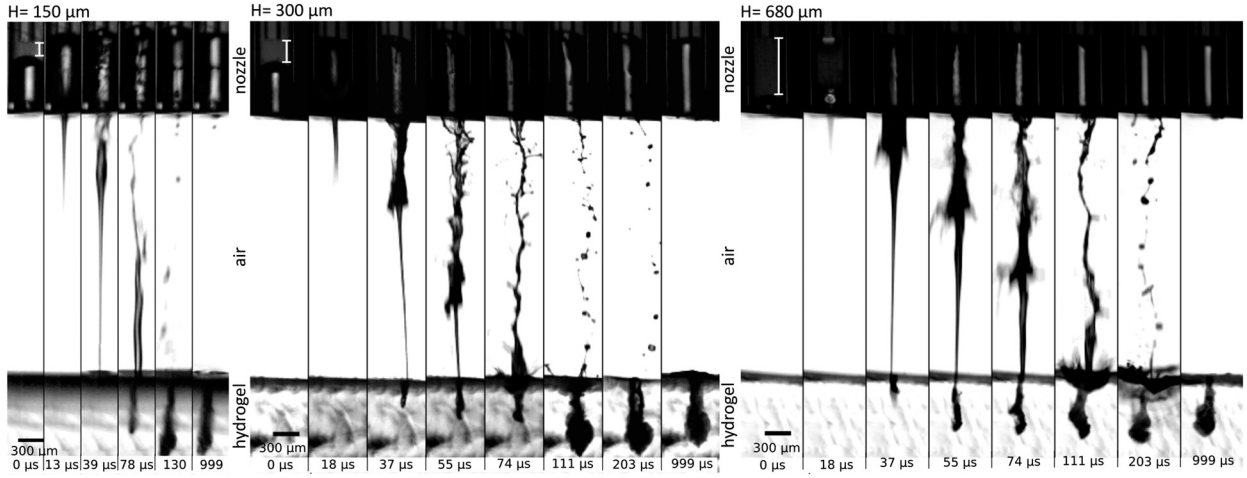

Fig. 5 Example of injection into a 1% agarose gel. Jets are propelled in different distances from the meniscus H (labelled with the white bar) but the energy is levelled so that they have similar velocities 130 m s^{-1}. Efficiency, as well as injected volume, vary with the actuation location. Distance between the nozzle and the meniscus is kept 3 mm for all cases.

different capillary diameters. Moreover, augmented volume injection can be achieved by implementing repetitive regime such as was shown in our previous work.[29]

3.3. Single drop regime

Cavitation in the low energy regime, slightly above the threshold, propels a single droplet. An extensive study of the different jetting regimes was made by Delrot *et al.*[31] with the system employing a microscope objective for the actuation from the side. Microdroplets can be printed with the sub-nozzle diameter and with high viscosity inks including non-Newtonian liquids. In the Fig. 6, we also demonstrate a single droplet generation with our endoscopic jet-injection device for three different capillary sizes (150 μm, 300 μm and 600 μm). In all cases, we used 105 μm fibre core size. Experiments were done with the 60% mass fraction of the glycerol in water stained with 52 mM concentration of Allura Red AC. The dynamic viscosity of the mixture was calculated by Cheng's empirical formula[43] as η = 9.2 cP. Results and parameters of the measurement are summarised in the Table 1. Printability and behaviour of liquid in motion can be evaluated by dimensionless Reynolds (Re), Weber (We) and Ohnesorge (Oh) numbers.[31,42,44] Typically, for a printing application inks have viscosities 2–15 cP and droplet velocities in the 3–10 m s^{-1} range.[44] The successful printing process is characterised by a single droplet without satellites and with velocity low enough to avoid splashing on a substrate. That falls into the region We < 200, Oh = 0.1–1.[44] Increase of the actuation energy leads to the ejection of bigger volumes but also contributes to the speed of the fluid and results in multiple droplets or a jet. Thus, to reliably change the droplet diameter one must change the capillary diameter. Table 1 shows change of the droplet diameter with respect to a capillary size. The result also represents the potential of fine dose control with nano-litre precision.

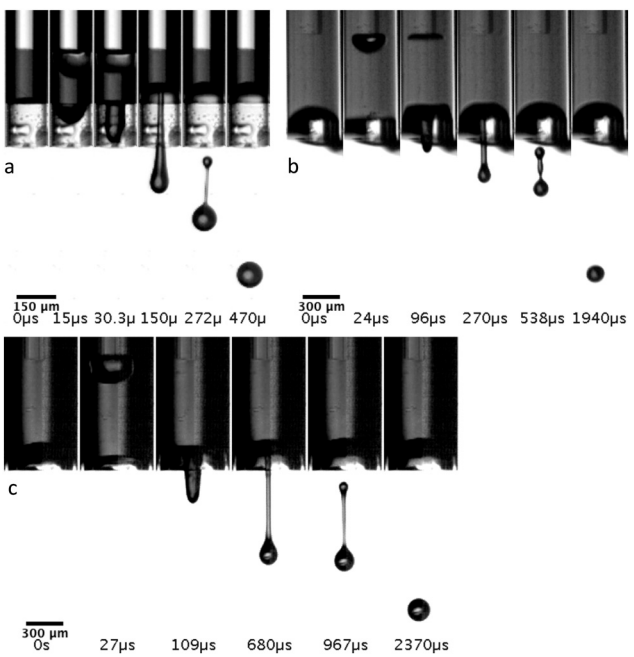

Fig. 6 Sequence of the single drop generation with a capillary diameter of a) 150 μm b) 300 μm and c) 600 μm.

3.4. Non-aqueous solutions

Laser-based jet injectors[21–30] were tested with aqueous solutions. While water is the most common solvent for

Table 1 Drop-on-demand regime results summary for different capillary diameters

D [μm]	E [μJ]	H [μm]	Speed [m s^{-1}]	Droplet diameter [μm]	Re	We	Oh
150	25.2 ± 1.2	190	4.3	99	34	20	0.13
300	36.1 ± 1.6	550	3.5	145	38	18	0.11
600	34.2 ± 1.5	650	4.5	207	64	39	0.10

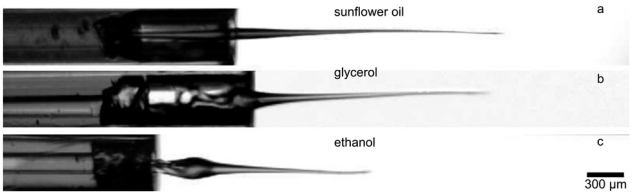

Fig. 7 Proof-of-the-concept for the most common pharmaceutically relevant solvents. a) Sunflower oil b) glycerol c) ethanol. Velocity in all cases is around 70 m s^{-1}.

injectable drugs, other fluids are frequently used as a solvent-vehicle for substances with poor solubility in water. In the Fig. 7 we present a proof of concept for the jet generation of the most common non-aqueous solvents – oil, glycerol and ethanol. Fluid properties like viscosity and surface tension do not play a role in the initial stage of the jet generation.[33,45] It was previously demonstrated that highly focused jets retain the laminar-like flow despite very high Reynolds numbers.[32] However, viscosity and surface tension are expected to have an impact on the formation of the slower tail.[46] In the slow single-drop regime, it was shown that the resulting regime (formation of either single drop, two drops or jet) is dependent on the viscosity.[31] Less viscous fluids with high surface tension (*e.g.* water) will more likely create small droplets and form the turbulent slower tail, whereas more viscous oils will be mostly dragged by the main stream of the jet (Fig. 7a). The liquid contained in a focused jet is in motion which is inertia-dominated, therefore the role of the density should be also considered.

3.5. Biocompatibility

Inks carrying biologically-relevant content are heat-sensitive, laser-induced jetting could potentially alter inks functionality. A previous study investigating this issue in a similar configuration[47] shows that the temperature rise is moderate (ΔT < 13 °C), spatially localized (<15 μm) and having a short time effect (<1.3 ms). Further studies employed laser-actuated cavitation in microfluidic systems in close vicinity of living cells.[48,49] Comparing these studies to our work, we use a laser energy that is one order of magnitude larger (<10 μJ in ref. 47, <1000 μJ in this study). However the fluence in our system is lower (<10 kJ cm^{-2} in ref. 47, <20 J cm^{-2} in this study). The volume affected by the direct laser illumination is larger but, because the fluence is lower, we hypothesize that its effect are not greater than reported in.[38–40] The ejection occurs in less than 5 μs so we can expect that the liquid in the front part of the jet will be intact due to a relatively long heat diffusion rate. Moreover, the vapor bubble occurs in a reasonable distance from the jet generation site and so the deposited fluid will not be affected. Another positive argument is that a similar system was used for bioprinting application of cell suspensions and authors showed good viability after processing of human umbilical vein endothelial cell.[50]

We assess the potential to deliver heat-sensitive biomolecules by testing the integrity of rabbit Immunoglobulin G (IgG) delivered with the endoscopic system on poly-L-lysine slides on which we performed an immunoassay test similar to the protocol in ref. 31 and 36. IgGs are large molecules with a strong structure–function relation[51] and their denaturation would result in losing affinity to the secondary antibody. Secondary antibodies are conjugated with Cy3 fluorescent dye and their presence on the slide is conditioned by binding to the primary antibody. Fig. 8 shows stains/droplets just after the deposition before drying and then fluorescent signal after performing the whole protocol. A patterned deposition allows us to see the clear contrast and the fluorescent signal shows the location of IgGs, which are not degraded by the ejection process. Measurements I–IV were made on the single slide and assessed under the same optical conditions to ensure comparable results. Measurements I and II represent jet generation under high laser energy (330 μJ) and with high velocity (>100 m s^{-1}), distance of the actuation site is 150 μm and 300 μm, with the total ejected volume approximately 14 nl and 24 nl, respectively. High velocity jet splashes on the substrate and create a stain of solution. We note that this jet would be injected in case of a softer material. Measurement III is the control matrix showing droplets deposited from the syringe without the laser actuation. Measurement IV was made with the mixture of primary antibodies which was held for 100 min in the 80 °C solution which should lead to the complete denaturation of the IgC molecules.[52] Indeed, we do not observe a fluorescent signal, proof that the secondary antibodies did not bind to the sites of the denaturized IgGs. Despite the positive outcome of this test, further assessment is needed as the effect on each molecule type can be different. Likely, the alteration and potential side products can occur in the proximity of the cavitation site and this might not be acceptable for a certain kind of application.

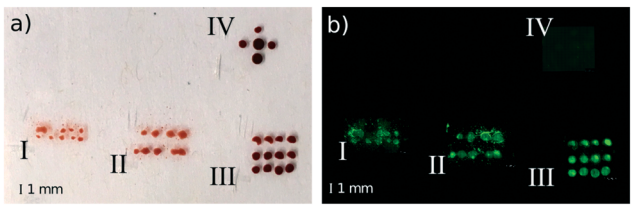

Fig. 8 a) Array of droplets/stains containing rabbit IgGs on the poly-L-lysine coated slide and b) the same array imaged in the fluorescent microscope after performing the immunoassay with fluorescent labelled secondary antibodies. Parameters of a droplet/stain generation: I. – laser pulse energy ≈ 330 μJ, laser fluence ≈ 3.8 J cm^{-2}, distance from the meniscus ≈ 150 μm, jet velocity ≈ 160 m s^{-1}, volume ejected ≈ 14 nl; II. – laser pulse energy ≈ 330 μJ, laser fluence ≈ 3.8 J cm^{-2}, distance from the meniscus ≈ 300 μm, jet velocity ≈ 130 m s^{-1}, volume ejected ≈ 24 nl; III. – no laser actuation, drops deposited from the syringe, volume ≈ 30 nl; IV. – no laser actuation, solution of denaturized primary IgGs. Presence of the fluorescence signal suggests that the functional properties of primary IgGs were not altered during the process of ejection. Scale bar in all images is equal to 1 mm.

Conclusions

We introduce an endoscopic fibre-based jet-injection device with is thin and long (*e.g.* 9.5 cm or 30 cm long, 1.2 mm in diameter) and thus easily implementable to catheters or other minimally invasive surgical systems. The actuation force is provided by a laser-induced cavitation bubble and light delivery is made through a thin multimode optical fibre. Our results suggest that the jet velocity is a function of the area over which the laser energy is distributed. A linear scaling of the jet velocity with the laser fluence is observed, which, in other words, means that the jet velocity scales with the inverse of the actuation area $v_{jet} \propto S^{-1}$. Optical fibres with smaller core generate faster jets as they intrinsically yield higher fluences by using the same pulse energy. The potential of our fibre-based delivery system for jet-injection is tested on soft tissue gel phantoms (1% agarose). We further show that the portion of injected liquid is dependent on the activation location in the capillary. We showed that our design implementation can achieve superior injection efficiency compare to systems using the side illumination, because the location of the actuation can be close enough to avoid slow and dispersed tail of the fluid. We tested the tool with a non-aqueous solutions and showed possible handling of oil, glycerol and ethanol based formulations. We further demonstrate the generation of low speed single droplets with parameters suitable for drop-on-demand printing or drug delivery with nanolitre precision. Finally, we demonstrate the potential of our device for delivery of heat-sensitive therapeutics by processing biomolecules (IgG) and showing their viability with an immunoassay.

Authors contribution

JK conducted experiments and wrote the manuscript. FdG contributed on building the set-up and participated on the study of velocity measurement. PD assisted to biocompatibility study and revised the manuscript. CM supervised the study and revised the manuscript.

Conflicts of interest

There are no conflicts to declare.

Acknowledgements

We would like to thank Prof. Konstantina Stankovic, MD, PhD, FACS (Harvard Medical School), Prof. Patrice Jichlinski, MD (CHUV Lausanne), Prof. George Wagnieres (LIFMET-EPFL) for insightful discussions about the application of the device. We acknowledge Prof. F. Gallaire (EPFL-LFMI) for lending us the high-speed camera. Finally, we thank Ugur Tegin for his help with optical fibre handling.

References

1 C. Dagdeviren, *et al.* Miniaturized neural system for chronic, local intracerebral drug delivery, *Sci. Transl. Med.*, 2018, **10**, eaan2742.
2 S. Ikemoto and L. G. A. Sharpe, Head-attachable device for injecting nanoliter volumes of drug solutions into brain sites of freely moving rats, *J. Neurosci. Methods*, 2001, **110**, 135–140.
3 E. E. Leary Pararas, D. A. Borkholder and J. T. Borenstein, Microsystems Technologies for Drug Delivery to the Inner Ear, *Adv. Drug Delivery Rev.*, 2012, **64**, 1650–1660.
4 M. Zanaty, T. Fussinger, A. Rogg, A. Lovera, D. Lambelet, I. Vardi, T. J. Wolfensberger, C. Baur and S. Henein, Programmable Multistable Mechanisms for Safe Surgical Puncturing, *J. Med. Devices*, 2019, **13**(2), DOI: 10.1115/1.4043016.
5 D. A. Fletcher, *et al.* Intravascular Drug Delivery With a Pulsed Liquid Microjet, *Arch. Ophthalmol.*, 2002, **120**, 3.
6 M. Kendall, Engineering of needle-free physical methods to target epidermal cells for DNA vaccination, *Vaccine*, 2006, **24**, 4651–4656.
7 W. Walther, *et al.* Intratumoral low-volume jet-injection for efficient nonviral gene transfer, *Mol. Biotechnol.*, 2002, **21**, 105–115.
8 W. Walther, I. Fichtner, P. M. Schlag and U. S. Stein, Nonviral Jet-Injection Technology for Intratumoral In Vivo Gene Transfer of Naked DNA, in *Gene Therapy of Cancer: Methods and Protocols*, ed. W. Walther and U. S. Stein, Humana Press, 2009, pp. 195–208, DOI: 10.1007/978-1-59745-561-9_11.
9 Y. Gong, *et al.* Needle-free injection of 5-aminolevulinic acid in photodynamic therapy for the treatment of non-melanoma skin cancer, *Dermatol. Ther.*, 2016, **29**, 255–262.
10 E. D. O'Cearbhaill, K. S. Ng and J. M. Karp, Emerging Medical Devices for Minimally Invasive Cell Therapy, *Mayo Clin. Proc.*, 2014, **89**, 259–273.
11 S. Mitragotri, Current status and future prospects of needle-free liquid jet injectors, *Nat. Rev. Drug Discovery*, 2006, **5**, 543–548.
12 P. Delrot, S. P. Hauser, J. Krizek and C. Moser, Depth-controlled laser-induced jet injection for direct three-dimensional liquid delivery, *Appl. Phys. A: Mater. Sci. Process.*, 2018, **124**, 616.
13 A. Arora, M. R. Prausnitz and S. Mitragotri, Micro-scale devices for transdermal drug delivery, *Int. J. Pharm.*, 2008, **364**, 227–236.
14 A. M. Römgens, *et al.* Penetration and delivery characteristics of repetitive microjet injection into the skin, *J. Controlled Release*, 2016, **234**, 98–103.
15 J. C. Stachowiak, *et al.* Piezoelectric control of needle-free transdermal drug delivery, *J. Controlled Release*, 2007, **124**, 88–97.
16 J. A. Simmons, *et al.* Characterization of skin blebs from intradermal jet injection: Ex-vivo studies, *J. Controlled Release*, 2019, **307**, 200–210.
17 J. W. McKeage, B. P. Ruddy, P. M. F. Nielsen and A. J. Taberner, Power-efficient controlled jet injection using a compound ampoule, *J. Controlled Release*, 2018, **291**, 127–134.
18 A. Taberner, N. C. Hogan and I. W. Hunter, Needle-free jet injection using real-time controlled linear Lorentz-force actuators, *Med. Eng. Phys.*, 2012, **34**, 1228–1235.
19 D. A. Fletcher and D. V. Palanker, Pulsed liquid microjet for microsurgery, *Appl. Phys. Lett.*, 2001, **78**, 1933–1935.

20 S. R. G. Avila, C. Song and C.-D. Ohl, Fast transient microjets induced by hemispherical cavitation bubbles, *J. Fluid Mech.*, 2015, **767**, 31–51.
21 C. B. Rodríguez, C. W. Visser, S. Schlautmann, D. F. Rivas and R. Ramos-García, Toward jet injection by continuous-wave laser cavitation, *J. Biomed. Opt.*, 2017, **22**, 105003.
22 T. Han, J. Hah and J. J. Yoh, Drug injection into fat tissue with a laser based microjet injector, *J. Appl. Phys.*, 2011, **109**, 093105.
23 H. Jang, *et al.* Towards clinical use of a laser-induced microjet system aimed at reliable and safe drug delivery, *J. Biomed. Opt.*, 2014, **19**, 058001.
24 V. Menezes, S. Kumar and K. Takayama, Shock wave driven liquid microjets for drug delivery, *J. Appl. Phys.*, 2009, **106**, 086102.
25 M. Moradiafrapoli and J. O. Marston, High-speed video investigation of jet dynamics from narrow orifices for needle-free injection, *Chem. Eng. Res. Des.*, 2017, **117**, 110–121.
26 M. Park, H. Jang, F. V. Sirotkin and J. J. Yoh, Er:YAG laser pulse for small-dose splashback-free microjet transdermal drug delivery, *Opt. Lett.*, 2012, **37**, 3894–3896.
27 H. Shangguan, L. W. Casperson, A. Shearin, K. W. Gregory and S. A. Prahl, Drug delivery with microsecond laser pulses into gelatin, *Appl. Opt.*, 1996, **35**, 3347–3357.
28 Y. Tagawa, N. Oudalov, A. El Ghalbzouri, C. Sun and D. Lohse, Needle-free injection into skin and soft matter with highly focused microjets, *Lab Chip*, 2013, **13**, 1357–1363.
29 J. Krizek, P. Delrot and C. Moser, Repetitive regime of highly focused liquid microjets for needle-free injection, *Sci. Rep.*, 2020, **10**, 5067.
30 C. Berrospe-Rodriguez, C. W. Visser, S. Schlautmann, R. Ramos-Garcia and D. Fernandez Rivas, Continuous-wave laser generated jets for needle free applications, *Biomicrofluidics*, 2016, **10**, 014104.
31 P. Delrot, M. A. Modestino, F. Gallaire, D. Psaltis and C. Moser, Inkjet Printing of Viscous Monodisperse Microdroplets by Laser-Induced Flow Focusing, *Phys. Rev. Appl.*, 2016, **6**, 024003.
32 Y. Tagawa, N. Oudalov, C. W. Visser, I. R. Peters, D. van der Meer, C. Sun, A. Prosperetti and D. Lohse, Highly Focused Supersonic Microjets, *Phys. Rev. X*, 2012, **2**(3), 031002.
33 I. R. Peters, Y. Tagawa, N. Oudalov, C. Sun, A. Prosperetti, D. Lohse and D. van der Meer, Highly Focused Supersonic Microjets: Numerical Simulations, *J. Fluid Mech.*, 2013, **719**, 587–605.
34 A. A. Manenkov, Fundamental mechanisms of laser-induced damage in optical materials: today's state of understanding and problems, *Opt. Eng.*, 2014, **53**, 010901.
35 B. C. Stuart, M. D. Feit, A. M. Rubenchik, B. W. Shore and M. D. Perry, Laser-Induced Damage in Dielectrics with Nanosecond to Subpicosecond Pulses, *Phys. Rev. Lett.*, 1995, **74**, 2248–2251.
36 M. Duocastella, J. M. Fernández-Pradas, J. L. Morenza, D. Zafra and P. Serra, Novel laser printing technique for miniaturized biosensors preparation, *Sens. Actuators, B*, 2010, **145**, 596–600.
37 A. Vogel, *et al.* Influence of optical aberrations on laser-induced plasma formation in water and their consequences for intraocular photodisruption, *Appl. Opt.*, 1999, **38**, 3636–3643.
38 P. K. Kennedy, D. X. Hammer and B. A. Rockwell, Laser-induced breakdown in aqueous media, *Prog. Quantum Electron.*, 1997, **21**, 155–248.
39 J. Noack and A. Vogel, Laser-induced plasma formation in water at nanosecond to femtosecond time scales: calculation of thresholds, absorption coefficients, and energy density, *IEEE J. Quantum Electron.*, 1999, **35**(8), 1156–1167.
40 A. Kiyama, *et al.* Visualization of penetration of a high-speed focused microjet into gel and animal skin, *J. Visualization*, 2019, **22**, 449–457.
41 A. Arora, *et al.* Needle-free delivery of macromolecules across the skin by nanoliter-volume pulsed microjets, *Proc. Natl. Acad. Sci. U. S. A.*, 2007, **104**, 4255–4260.
42 L. Oyarte Gálvez, *et al.* Microfluidics control the ballistic energy of thermocavitation liquid jets for needle-free injections, *J. Appl. Phys.*, 2020, **127**, 104901.
43 N.-S. Cheng, Formula for the Viscosity of a Glycerol–Water Mixture, *Ind. Eng. Chem. Res.*, 2008, **47**, 3285–3288.
44 B. Derby, Inkjet Printing of Functional and Structural Materials: Fluid Property Requirements, Feature Stability, and Resolution, *Annu. Rev. Mater. Res.*, 2010, **40**, 395–414.
45 A. Antkowiak, N. Bremond, S. Le Dizès and E. Villermaux, Short-term dynamics of a density interface following an impact, *J. Fluid Mech.*, 2007, **577**, 241.
46 J. Eggers and E. Villermaux, Physics of liquid jets, *Rep. Prog. Phys.*, 2008, **71**, 036601.
47 P. A. Quinto-Su, M. Suzuki and C.-D. Ohl, Fast temperature measurement following single laser-induced cavitation inside a microfluidic gap, *Sci. Rep.*, 2014, **4**, 5445.
48 Z. G. Li, A. Q. Liu, E. Klaseboer, J. B. Zhang and C. D. Ohl, Single cell membrane poration by bubble-induced microjets in a microfluidic chip, *Lab Chip*, 2013, **13**, 1144–1150.
49 P. A. Quinto-Su, C. Kuss, P. R. Preiser and C.-D. Ohl, Red blood cell rheology using single controlled laser-induced cavitation bubbles, *Lab Chip*, 2011, **11**, 672–678.
50 H. Ebrahimi Orimi, *et al.* Drop-on-demand cell bioprinting via Laser Induced Side Transfer (LIST), *Sci. Rep.*, 2020, **10**, 9730.
51 A. W. Vermeer and W. Norde, The thermal stability of immunoglobulin: unfolding and aggregation of a multi-domain protein, *Biophys. J.*, 2000, **78**, 394–404.
52 Y. Akazawa-Ogawa, H. Nagai and Y. Hagihara, Heat denaturation of the antibody, a multi-domain protein, *Biophys. Rev.*, 2018, **10**, 255–258.
53 K. Cu, R. Bansal, S. Mitragotri and D. F. Rivas, Delivery Strategies for Skin: Comparison of Nanoliter Jets, Needles and Topical Solutions, *Ann. Biomed. Eng.*, 2020, **48**(7), 2028–2039.